Biosensors and Bioelectronics 126 (2019) 178–186

Contents lists available at ScienceDirect

Biosensors and Bioelectronics

journal homepage: www.elsevier.com/locate/bios

A SERS microfluidic platform for targeting multiple soluble immune checkpoints

K.Kamil Reza[a], Abu Ali Ibn Sina[a,*], Alain Wuethrich[a], Yadveer S. Grewal[a], Christopher B. Howard[c], Darren Korbie[a], Matt Trau[a,b,**]

[a] Centre for Personalised Nanomedicine, Australian Institute for Bioengineering and Nanotechnology (AIBN), The University of Queensland, Corner College and Cooper Roads (Bldg 75), Brisbane, QLD 4072, Australia
[b] School of Chemistry and Molecular Biosciences, The University of Queensland, Brisbane, QLD 4072, Australia
[c] Centre for Advanced Imaging (CAI), University of Queensland, Brisbane, Australia

ARTICLE INFO

Keywords:
Immune checkpoints
Cancer
SERS
ac-EHD
Microfluidic device

ABSTRACT

Immune checkpoint blockade therapies are promising next generation immunotherapeutic treatments for cancer. Whilst sequential solid biopsies are an invaluable source of prognostic information, they are not feasible for monitoring therapeutic outcomes over time. Monitoring soluble immune checkpoint markers expression in body fluids could potentially be a better alternative. Current methods (e.g. ELISA) for detecting immune-checkpoint proteins mostly rely on the use of monoclonal antibodies which are expensive and time-consuming to manufacture and isolate. Herein, we report an integrated surface enhanced Raman scattering (SERS)-microfluidics device for the detection of immune checkpoint proteins which involves the use of i) nano yeast single chain variable fragment (scFv) as a promising alternative to monoclonal antibodies providing high stability at relative low-cost and simplicity for production, ii) graphene oxide functionalised surface to reduces the bio functionalization steps, thus avoiding the general paradigm of biotin-streptavidin chemistry and iii) a microfluidic platform enabling alternating current electrohydrodynamics (ac-EHD) induced nanomixing to enhance the target scFv binding and minimize the non-specific interactions. Specific and multiplex detection of immune checkpoint biomarkers is achieved by SERS based spectral encoding. Using this platform, we successfully demonstrated the detection of clinically relevant soluble immune checkpoints PD-1, PD-L1 and LAG-3 from as low as 100 fg/mL of analytes spiked in human serum.

1. Introduction

Immune checkpoints are the key regulatory part of the immune system by which T-cells recognise host cells and thereby maintains homeostasis and prevent autoimmunity (Joller et al., 2012; Karin et al., 2006; Sakaguchi, 2004). In cancer, tumour cells use this molecular mechanism of immune suppression to resist antitumor immune response and escape from the cell apoptosis system (Alme et al., 2016; Pardoll, 2012; Postow et al., 2015; Wherry, 2011). For instance, the interaction of the programmed cell death-1 (PD-1) and lymphocyte activation gene-3 (LAG-3) receptor of T-cells with the programmed cell death ligand-1 (PD-L1) and the major histocompatibility complex (MHC) class II molecules of the tumour cells respectively are found to be the most common methods used by tumour cell to suppress the T cell activity.(Huang et al., 2015b; Iwai et al., 2002). One strategy to avoid this immunosuppression is to selectively inhibit/block the immune checkpoints interactions which can restore and promote T-cell survival and proliferation (Nagato et al., 2017). Immune checkpoint blockade therapy has therefore been found to be instrumental for the treatment of cancer (Anderson et al., 2016; Huang et al., 2015b; Sharma and Allison, 2015). However, monitoring the therapeutic outcome is still challenging and requires invasive methods. Soluble immune checkpoint markers which are released from the tumour/T-cell into the circulatory system can provide a possible solution for non-invasive monitoring of the patient response towards treatment (Shi et al., 2013). Moreover, not all cancer patients respond to the same therapy, as such a multiplex soluble immune checkpoints platform could facilitate simultaneous monitoring of multiple immune checkpoints and suggest effective

* Corresponding author.
** Corresponding author at: Centre for Personalised Nanomedicine, Australian Institute for Bioengineering and Nanotechnology (AIBN), The University of Queensland, Corner College and Cooper Roads (Bldg 75), Brisbane, QLD 4072, Australia.
E-mail addresses: a.sina@uq.edu.au (A.A.I. Sina), m.trau@uq.edu.au (M. Trau).

https://doi.org/10.1016/j.bios.2018.10.044
Received 16 July 2018; Received in revised form 28 September 2018; Accepted 18 October 2018
Available online 25 October 2018
0956-5663/

therapy for individual patients (Koyama et al., 2016).

The detection of immune checkpoint markers in complex samples is currently facilitated by specific avidity reagents such as monoclonal antibodies (mAbs) (Scott et al., 2012). However, the production and isolation of antibodies is laborious and the antibody efficacy is often affected by the storage conditions that generally requires refrigeration for long time storage (Grewal et al., 2016). Recombinant antibody-like molecules such as single chain variable fragment (scFv) have emerged as cost-efficient alternative to monoclonal antibodies which could be rapidly isolated from various display technologies such as yeast display (Holliger and Hudson, 2005). While scFvs shows excellent activity on yeast surfaces, they lose their efficacy very often in solution. Our group has recently developed a scFv based affinity reagent called nanoyeast scFv (NY-scFv) which addressed these limitations and successfully used as an alternative to monoclonal antibodies in detecting clinically relevant biomolecules,(Vaidyanathan et al., 2015; Wang et al., 2014)'(Grewal et al., 2015).

Surface-enhanced Raman scattering (SERS) is an excellent readout technique for detecting biomolecules, and have gained wide attention as an alternative to fluorescence based immune-platform due to its multiplexing capability and photostability (Huang et al., 2015a; Laing et al., 2016; Luo et al., 2014; Qian and Nie, 2008; Wang et al., 2017). However, the major limitations of SERS based immune-platform are the less antibody- target interaction due to the slow diffusion of SERS nanoparticles and the high level of nonspecific attachment of biomolecules towards the sensor surface. To address this limitation, we have recently developed a SERS-microfluidic platform which utilizes alternating current electrohydrodynamic (ac-EHD) fluid flow thus avoiding the use of any external pump. This ac-EHD induced fluid flow generates a nanoscale shear force at the double layer of the sensing electrodes which significantly increases the antibody-target binding and at the same time shears off the non-specifically bound molecules from the sensor surface (Reza et al., 2017; Wang et al., 2015). Despite this advantages, this method utilized biotin-streptavidin chemistry followed by immune-affinity approach using monoclonal antibody which limits its application in clinical settings.

Herein, we report a SERS-microfluidic immune checkpoint detection platform that utilized graphene oxide (GO) and NY-scFv affinity reagent modified surface functionalisation to capture the target molecules. The use of NY-scFv provides several advantages over monoclonal antibodies as it is cost effective, easy to manufacture and temperature stable for long time. The use of GO functionalisation obviates the need for biotin-streptavidin chemistry and thereby provides rapid analysis by reducing the functionalisation steps in comparison to the previous methods (Chen et al., 2012; Pumera, 2011; Reza et al., 2015; Wang et al., 2011). The assay also used an ac-EHD induced surface shear forces that increases the sensitivity and specificity due to the increase of NY-scFv-target interaction and removal of the non-specific adsorption of biomolecules towards sensor surface. Finally, the detection with SERS provides multiplexing capacity without photo bleaching, a common limitation of fluorescence based methods. Using this platform, we show that the assay is highly specific in detecting immune checkpoint markers (i.e. PD-1, PD-L1 and LAG-3) with negligible non-specific signal. We also demonstrate the applicability of this platform in detecting as low as 100 fg/mL PD-1, PD-L1, and LAG-3 spiked in serum. Moreover, by utilizing the multiplexing capacity of SERS, we successfully detect the all three immune-checkpoint protein from a complex serum sample when passed through a single channel functionalized with respective NY-scFvs. We believe that this method will provide a significant improvement in the current clinical system for disease diagnosis and therapeutic monitoring.

2. Materials and methods

2.1. Reagents

All reagents including antibodies, antigens were obtained from Sigma-Aldrich (Australia), Novusbio (Australia), R&D/Life Technologies (Burlington, ON), Thermo-Fisher Scientific (Australia), BBI Solutions system, Santa Cruz Biotech (Australia), Astral Scientific (Australia) and Invitrogen (Australia). All reagents and washing solutions used in the experiments were prepared using phosphate buffer saline (PBS, 1 mM, pH 7.4). Stock solutions of antibodies were diluted in PBS. Photoresists for fabrication (MicroChem, Murphys, CA) were used according to the manufacturer's instruction.

2.2. Preparation of SERS nanotags

The SERS nanotags were prepared by the same method as described by our previous studies (Kamil Reza et al., 2017). The gold nanoparticles were synthesized by citrate reduction of $HAuCl_4$ as reported in literature.(Frens, 1973) The mixture of 2 μL of 1.0 mM DSP (dithiobis succinimidyl propionate) in DMSO (dimethyl sulfoxide) and Raman reporters (either 5 μL of 1 mM MBA (mercaptobenzoic acid), 10 μL of 1 mM DTNB ((5,5′-dithio-bis-[2-nitrobenzoic acid]), 10 μL of 1 mM MMC (7-mercapto-4-methylcoumarin), in ethanol were incubated with 1.0 mL of AuNPs overnight to form a mixed thiol monolayer on gold nanoparticle surface. Next, the colloid was centrifuged at 7600 rpm for 10 min to remove the residual reactants and then resuspended in 200 μL PBS buffer. Next, 2 μg either human anti-PD-1, anti-PD-L1, anti-LAG-3, antibodies or isotype-matched immunoglobulin (IgG) control was added to the colloid with 0.5 h incubation time at room temperature. After that, the colloid was centrifuged at 7600 rpm at 4 °C for 8 min to remove the free antibodies and resuspended in 200 μL of 0.1% BSA for 0.5 h at room temperature which act as stabilising agent and also minimize the non-specific adsorption.

2.3. Device fabrication

The nanoshearing chip was fabricated using standard photolithography procedures and PDMS channels were fabricated using soft lithography technique (Supplementary Fig. S1 and S2). The chip was sandwiched between custom-built holders to introduce inlets and outlets for the reagents and sample run. The electrode patterns were designed in Layout Editor (L-Edit V15, Tanner Research Inc., CA) and printed on a chrome mask (5 in. × 5 in.) obtained from Qingyi Precision Mask-making (Shenzhen) Ltd., China. The device contains asymmetric planar microelectrode pairs within a long microchannel. The device contains five channels with individual inlet and outlet ports with each channel composed of 50 asymmetric planar electrode pairs (dimension of small and large electrode are 100 μm and 400 μm, separation between electrodes is 100 μm). Adjacent electrode pairs in each segment are separated by a distance of 150 μm. The small and large electrodes were connected to a larger gold pads to form the electrical connections. We have used 4-in. silicon wafers. Firstly, silicon dioxide (thickness, 200 nm) was deposited on silicon wafers (diameter, 100 mm; thickness, 1 mm; single-side polished) in an oxidation furnace to active passivation. The oxidised wafers were cleaned with acetone for 5 min under sonication, then rinsed with isopropyl alcohol and water for another 2 min and dried under nitrogen gas. To obtain a thick layer of resist, negative photoresist (AZnLOF 2070, MicroChem, Newton, MA) was spin coated (3000 rpm for 30 s) onto the wafer and soft baked at 110 °C for 6 min. Subsequently, these wafers were exposed to UV (280 mJ/cm^2) using a mask aligner (EVG 620, EV Group GmbH, Austria) and development was done using AZ 726 developer (for 3 min), revealed the exposed patterns. Then the chips were rinsed with deionized (DI) water and dried under nitrogen gas. The metallic deposition (Ti (10 nm) and Au (200 nm)) onto chip was carried out using

an electron beam (e-beam) evaporator (Temescal FC-2000) under high vacuum conditions followed by lift-off using ethanol exposing the patterned gold electrodes. Finally, the wafers were then diced (ADT 7100 wafer precision dicer) to obtain individual devices.

The fabrication of microfluidic channels involves fabrication of an SU-8 master molds containing five independent microfluidic channels (width, w = 400 μm; height, h = 300 μm; length, l = 25 mm) with 1 mm diameter inlet and outlet ports. The fabrication of microfluidic channels on PDMS using the master molds were described here. Briefly, a thick layer of negative photoresist (SU-8 2150; MicroChem, Newton, MA) was spin coated (1800 rpm) onto a clean silicon wafer. The wafer was soft baked through a series of step changes in temperature (65 °C for 7 min, 95 °C for 60 min, 65 °C for 5 min). Subsequently, UV exposure (380 mJ/cm^2) was followed by a post bake step (from 65 °C for 5 min, 95 °C for 20 min, 65 °C for 3 min). To expose the fluidic channels, the wafers were developed in propylene glycol methyl ether acetate (PGMEA) for 45 min. To prepare the channels, PDMS precursor was mixed with the curing agent (ratio 10:1; Sylgard 184 kit, Dow Corning, Midland, MI), degassed and allowed to cure in a conventional oven at 65 °C for 2 h. The cured PDMS replicas were removed from the molds and 1 mm holes were punched into PDMS at either ends of the channel to define the inlet and outlet ports (diameter, 1 mm).

2.4. Generation of nanoyeast-scFv

PD1, PDL-1 and LAG-3 whole yeast scFv and nanoyeast-scFv were produced as per the method detailed in this work (Li et al., 2018). To check the specificity of NY-scFvs, we performed ELISA and found that all the target scFvs have high affinities towards the target antigen (Supplementary Fig. S3).

2.5. Multiplexed ac-EHD SERS Immunoassay

The fabricated chips were cleaned with acetone, ethanol and water and then dried with nitrogen gas and stored under sealed vacuum. The electrodes were then functionalized with GO following a method where a self-assembled monolayer of n-octadecyl mercaptan were used for absorption of the nanosheets.(Yang et al., 2010) In this way, we efficiently fabricated the graphene gold conjugate with a controllable surface coverage of GO. The GO functionalized device was then bonded to the PDMS containing the channels and the device was sandwiched between custom-built holders and fixed into a microfluidic platform. This step was then followed by HA antibody functionalization in separate channels of the device using standard EDC-NHS chemistry (EDC: 0.2 M; NHS: 0.05 M; mixing volume ratio of 1: 1)(Ali et al., 2014). NY-scFv specific anti-PD-1 affinity agents (10 μg/mL) was immobilized with the use of a human influenza hemagglutinin (HA) antigen tag cloned into the recombinant scFv construct at room temperature for 1 h leading to the immobilization of the antibody onto the GO functionalized gold surface. Thus, this assay uses anti-HA antibody to build immunoassays using yeast-scFvs selected to bind antigens of interest. Similarly, we also functionalized other channels with NY-scFv specific anti-PD-L1 and anti- LAG-3 affinity agents at a concentration of 10 μg/mL using the same method. Afterwards, 1% BSA solution was passed through each of the channels to block the nonspecific adsorption. Supplementary Fig. S4 showed the schematic illustration of the GO ac-EHD immunoassay.

Samples containing target proteins in serum were then driven under optimized ac-EHD condition (f = 1.1 kHz and V_{pp} = 120 mV). Upon capture, targets were detected using samples containing SERS-labelled antibody (anti-PD-1) and/or antibodies (anti-PDL-1, anti-LAG-3) driven through the capture domain under similar electric field condition. For clinical sample analysis, patient serum samples were obtained from Ventyx Wesley Research Institute Tissue Bank (Brisbane, Australia). Samples were collected and stored at −80 °C.

2.6. SERS measurement and data analysis

SERS spectra and images were recorded with a Witec alpha 300R microspectrometer. The 632.8 nm line from a HeNe laser with a laser power of 4 mW on the sample was used for excitation of Raman scattering (Zeman and Schatz, 1987). The resolution for the Raman microspectrometer is 2 cm^{-1}. The integration time of the SERS was 100 ms, with a mapping an area of 60 μm × 60 μm (60 pixel × 60 pixel) using a 20 × microscope objective. A silicon wafer was used for calibration of the system based on the Raman intensity of the first-order photon peak of silicon at ~ 520 cm^{-1}. We also performed background removal from the raw spectra was done using a Vancouver Raman Algorithm based on a fifth-order polynomial fitting method (Zhao et al., 2007). In order to reduce the error and improve the preciseness of the measurement, we scanned multiple positions on different electrodes in each channel. Each set of experiments were repeated thrice. Finally, average Raman intensities of the targets were obtained from these images from three different spectra for each sample (used the peak height to plot the intensity bar).

3. Results and discussion

3.1. Immune checkpoint platform

To demonstrate the assay platform, we constructed an ac-EHD enabled microfluidic device (Fig. 1, see experimental section for detail fabrication steps) containing asymmetric pairs of large and small electrodes (Supplementary Fig. S1 and S2) using our previously developed method (Kamil Reza et al., 2017). The application of an alternating potential difference across large and small asymmetric electrode pair results in a non-uniform electric field that induces charges within the double layer of each electrode. The lateral variation in the total amount of induced double layer charges and spatial distribution of charges on the electrode surface, give rise to a stronger lateral forces on the large electrode resulting in a net fluid flow towards the large electrode. This surface shear force is unidirectional and generates within few nanometers of the sensing surface. Consequently, this surface shear force drags the analytes in solution towards the flow and their mixing with the surface improves better interaction of antibody-antigen.

Fig. 1 shows the schematic illustration of the assay. The ac-EHD device was first functionalized with GO followed by the Hemagglutinin (HA) antibody using EDC/NHS chemistry (1-Ethyl-3-(3-dimethylaminopropyl)-carbodiimide)/(N-hydroxysuccinimide). Next, PD-1, PDL1 and LAG-3 specific NY-scFvs which have HA antigen tag were attached to the functionalised HA antibody. The sample containing immune-checkpoint antigens were then injected into the different channels of the ac-EHD device consisting of an array of PD-1, PD-L1 and LAG-3 specific NY-scFv and GO functionalized gold electrode pairs. An ac-field was then applied to the GO coated gold electrode arrays which resulted in an EHD-induced fluid flow and generated delicate micro-mixing within few nanometers of the electrode surface (Supplementary Fig. S3). Another channel was not functionalized with the NY-scFv to act as a negative control. Samples (20 μL) containing soluble immune checkpoints in serum were driven through functionalized devices using optimized ac-EHD conditions (f = 1.1 kHz and V_{pp} = 120 mV) to facilitate specific target capture. Subsequently, the captured antigens were detected using three different SERS nanotags. SERS nanotags were synthesized using gold nanoparticles of size 60 nm conjugated with detection antibody and Raman reporters. The Raman reporters with their characteristic peaks are specific to the three target biomarkers. (e.g., MBA at 1074 cm^{-1} for PD-1, DTNB at 1337 cm^{-1} for PD-L1, and MMC at 1175 cm^{-1} for LAG-3) respectively. We utilized spatially resolved microspectroscopic SERS detection system and scanned multiple positions of each electrodes to acquire an average spectra of each biomarker.

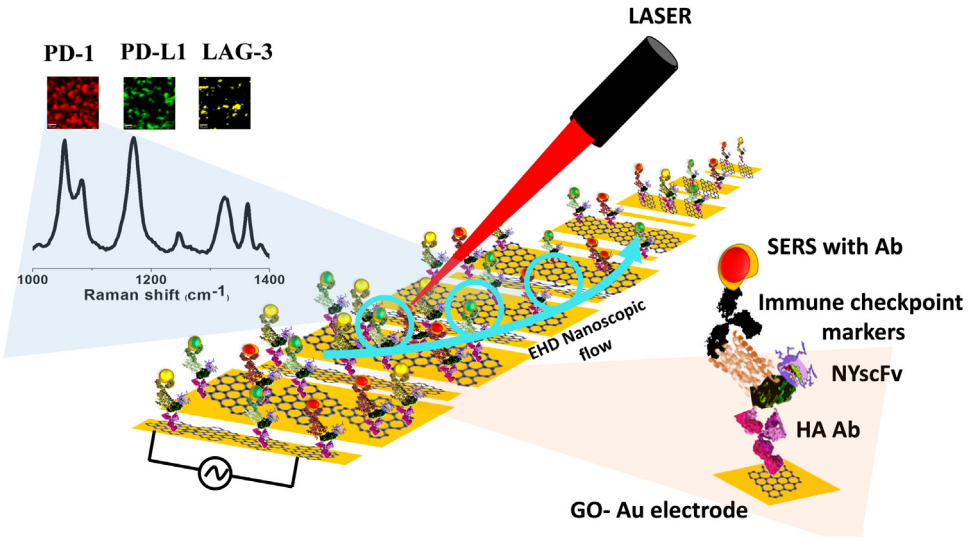

Fig. 1. Schematic illustration of the SERS GO ac-EHD immunoassay for immmuno checkpoint blockade biomarkers.

3.2. Initial investigation on GO and NY-scFv functionalised surface

Graphene oxide has become very popular in biosensing due to its larger surface area which could allocate large number of antibodies directly into the sensor surface. In this way, we reduce the multiple functionalization steps of standard biotin-streptavidin procedure of antibody functionalization on any surface. To confirm the GO functionalization on gold surface, we carried out Raman studies of gold electrode and GO coated gold electrode (Fig. 2a). The two characteristics peaks of GO are D and G band confirms the functionalization of GO on gold electrode.

Further, we carried out scanning electron microscopy (SEM), bright-field microscopy and differential pulse voltammetry (DPV) studies of the electrodes to show morphological differences of these electrodes. As shown in Fig. 2(b) and (c), the modification of the (i) bare gold surface with (ii) graphene oxide caused a visible change in the bright field image (c (i-iii)) and increased the electrode surface roughness, as clearly indicated by the SEM images (b (i-ii)). The morphology change of the modified electrode is likely to be a result of the formation of graphene oxide layers on the gold surface. The conjugation with

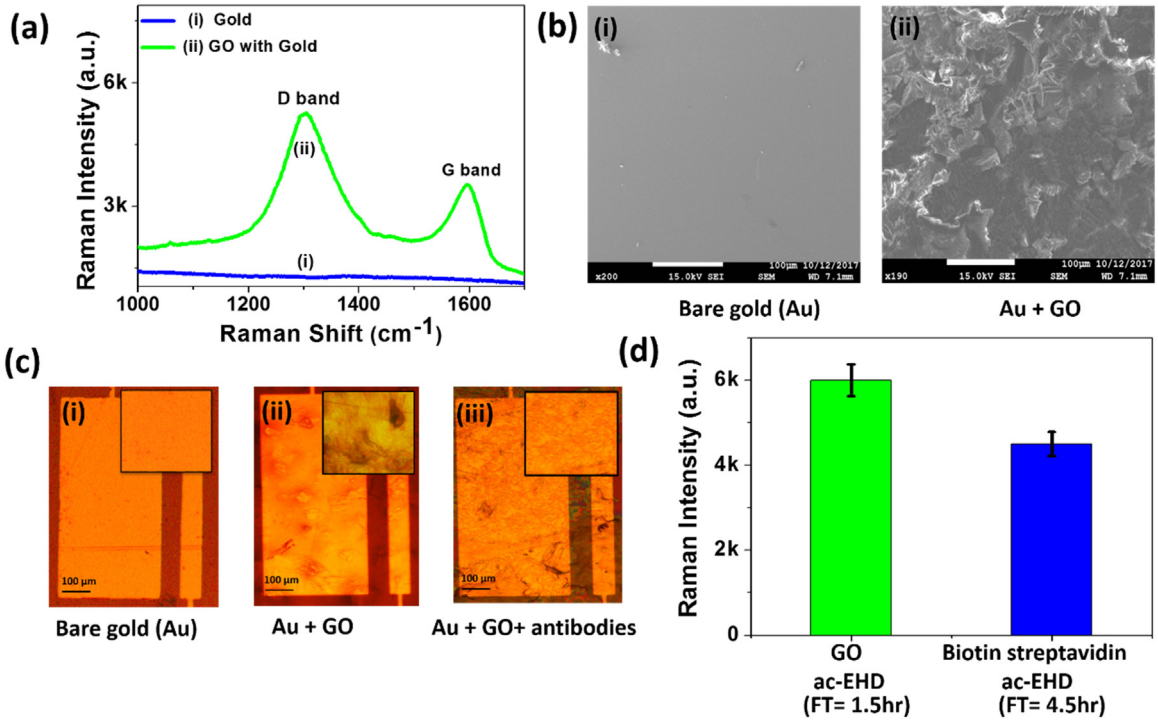

Fig. 2. (a) Raman spectra of gold electrodes and graphene oxide functionalised gold electrodes. [b (i-ii)] The SEM images of the bare gold electrode (Au) and gold electrode with graphene oxide coating (Au + GO). [c (i-iii)] The microscopic images of (i) the gold electrode (Au) (insets show the magnification), (ii) gold with graphene oxide (Au + GO) and (iii) gold with graphene oxide, HA ab and nanoyeast (PD-1) (Au + GO + antibodies). (d) Comparison between (i) graphene oxide (green bar) and (ii) biotin-streptavidin (blue bar) functionalized electrodes where the bar graphs show the average SERS intensity for the detection of HER2 protein using anti-HER-2 functionalised electrodes. The antibody functionalization time (FT) for graphene oxide ac-EHD assay is 1.5 h and biotin-streptavidin ac-EHD assay is 4.5 h respectively. Each data point represents the average of three separate trials (n = 3) and error bars represent the standard deviation of measurements within each experiment. (For interpretation of the references to color in this figure legend, the reader is referred to the web version of this article.).

biomolecules could not be characterised by microscopy, thus we carried out an electrochemical study (Supplementary Fig. S5). To monitor the stepwise electrode modification, we carried out electrochemical measurements using differential pulse voltammetry (DPV) with ferro/ferricyanide redox couple. The successful electrode modification is indicated by a decrease in DPV peak signal with every modification step. Fig. S5(a) shows the stepwise functionalisation. Initially, the (i) DPV signal of the unmodified bare gold electrode was measured. Subsequently, the electrode was modified with layers of (ii) graphene oxide, (iii) HA antibody, (iv) PD-1 nanoyeast, and (v) PD-1 antigen. Each of these steps resulted in a DPV signal decrease suggesting the successful biosensor preparation. In Fig. S5(b), a magnification of the inset in (a) with the DPV signals (ii-v) is shown for clarity.

To show the comparison in sensitivity of the GO and biotin streptavidin system, we functionalized two chips with HA antibody followed by NY-scFv on both devices and flew PD-1 antigen (1 pg/mL) under ac-EHD conditions (f = 1.1 kHz and V_{pp} = 120 mV). In the first chip, HA antibody followed by NY-scFv was coated on to GO gold surface using EDC-NHS chemistry, while in the second chip, same amount of HA antibody and NY-ScFv was coated onto gold surface using biotin-streptavidin process. The Raman intensities obtained from GO ac-EHD (green bar) is higher than the biotin streptavidin ac-EHD gold surface (blue bar) with less antibody functionalization time (FT), providing a simple and quicker way (Fig. 2d) of functionalization.

3.3. Assay specificity study

Fig. 3 shows the detection specificity of the immune checkpoint assay. The corresponding false colour SERS images are shown in Supplementary Fig. S6. The specificity was investigated in human serum as a relevant example of a clinical sample. Aliquots of serum were spiked separately with 10 pg/mL immune checkpoint markers (positive control) or with 1 ng/mL non-target protein IgG (negative control). The human serum samples could contain

trace concentrations of PD-1, PD-L1, and LAG-3. To assess for a detection bias due to the potential presence of these targets, the blank serum sample (without spiking) was also analysed as control. The samples were run through the device channels under an applied ac-EHD field of f = 1.1 kHz and V_{pp} = 120 mV. As shown in Fig. 3, at a target concentration of 10 ng/mL, a strong SERS signal was obtained for all three immune checkpoint markers as can be seen from the SERS spectra and false-colour SERS images. The NY-scFv affinity reagents were crucial for successful target capture. In the absence of the NY-scFv (no scFv), PD-l, PD-L1, and LAG-3 could not be detected. All the negative control samples provided negligible signals. This data suggests that the immuno-capture was highly specific using the NY scFv integrated on the SERS ac-EHD device.

3.4. Assay sensitivity and dynamic range

To investigate the sensitivity and dynamic range of detection, serum

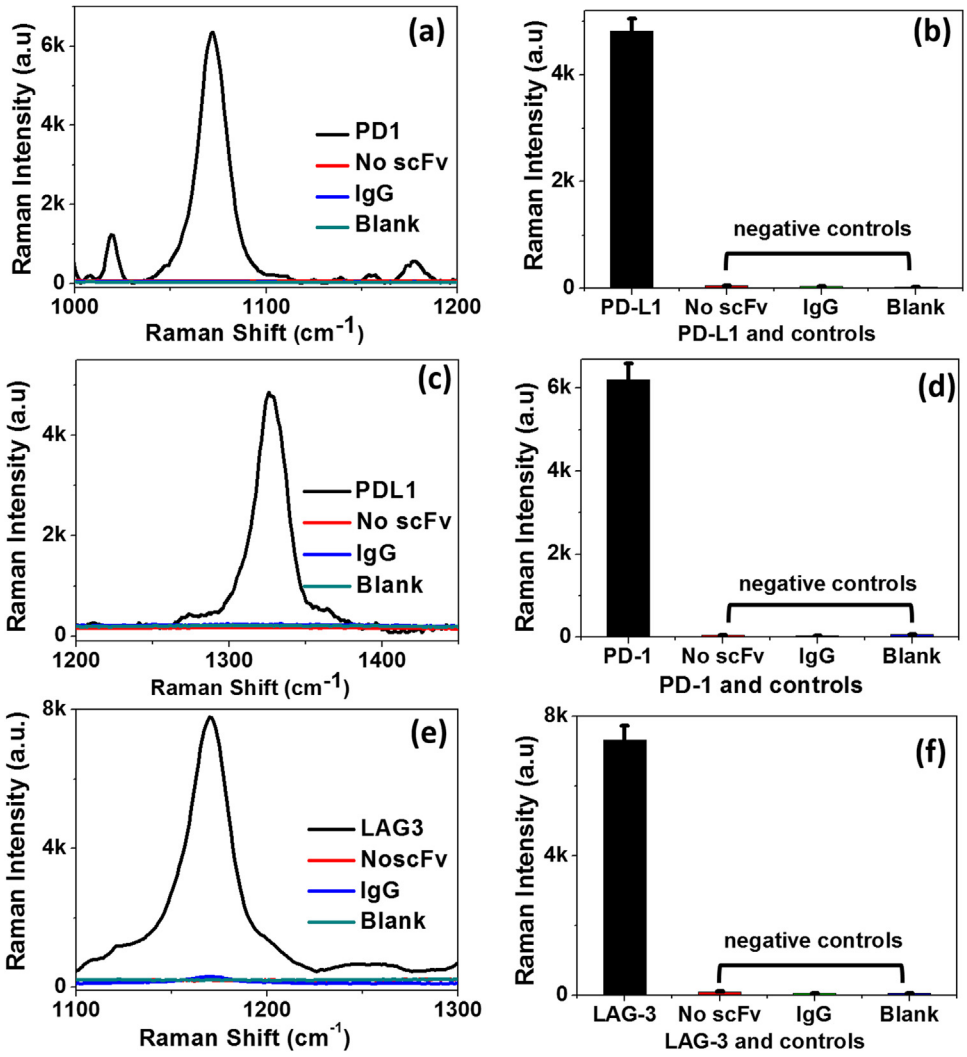

Fig. 3. Assay specificity study for immune-checkpoint biomarkers in human serum. The SERS spectra and average SERS intensities are shown for (a, b) PD-1 (peak at 1074 cm^{-1}), (c,d) PD-L1 (peak at 1337 cm^{-1}), and (e, f) LAG-3 (peak at 1174 cm^{-1}). The samples were spiked with 10 pg/mL target antigen (black), target antigen without scFv (negative control, red), 1 ng/mL non-target IgG (negative control, blue), and blank serum (negative control, green). Each data point in (b, d, and f) represents the average of three separate trials *(n = 3)* and error bars represent standard deviation (%RSD = < 5% for n = 3) of measurements within each experiment. (For interpretation of the references to color in this figure legend, the reader is referred to the web version of this article.).

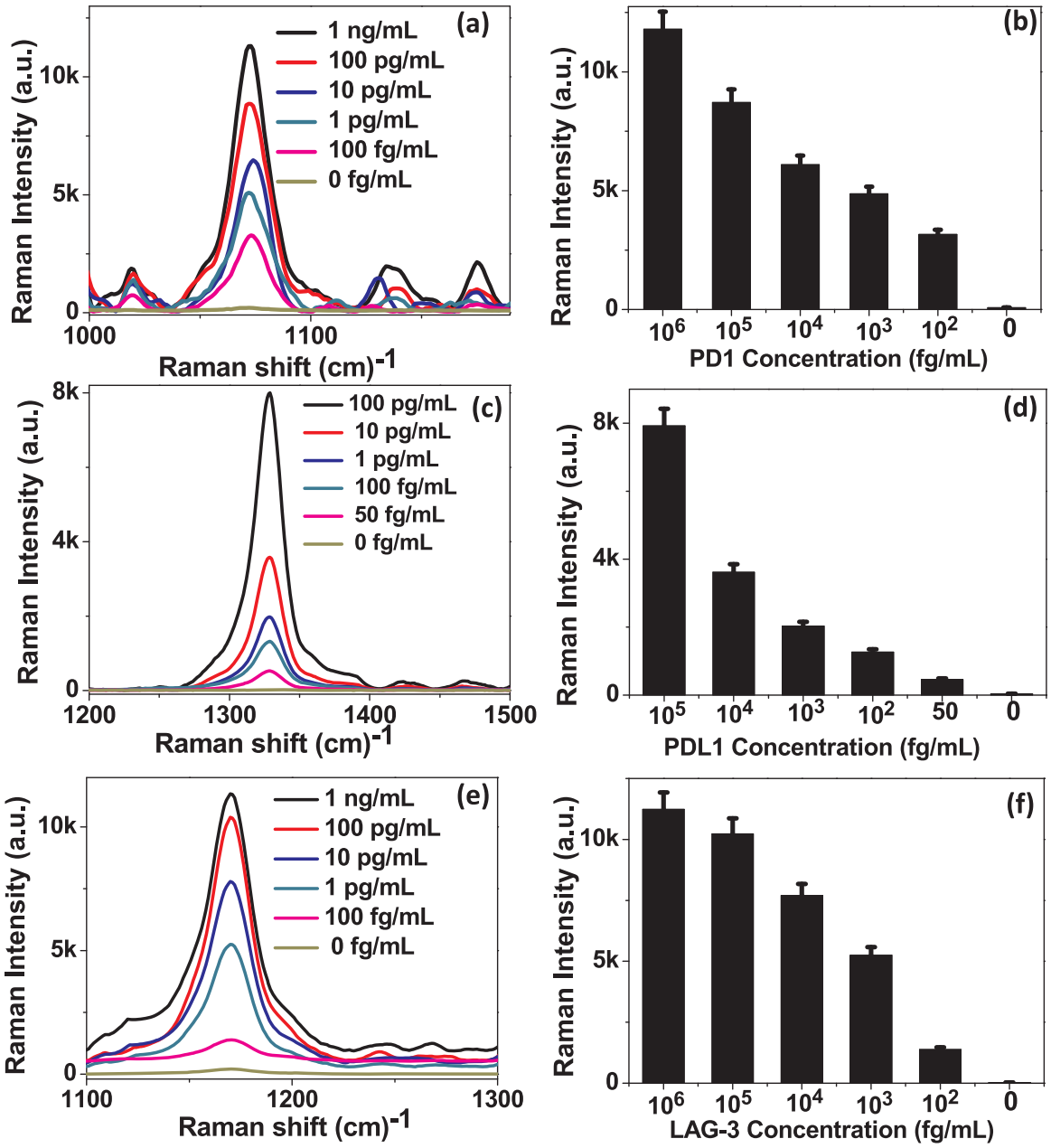

Fig. 4. Typical SERS spectra and dynamic range for PD-1 (a and b), PD-L1 (c and d) and LAG-3 (e and f). The serum samples spiked with targets were run through the device under an ac-EHD field (f = 1.1 kHz and V_{pp} = 120 mV). Control experiments were performed using blank serum samples (0 fg/mL). Each data point in (b), (d) & (f) represents the average of three separate trials *(n = 3)* and error bars represent standard deviation (%RSD < 3.65% for n = 3) of the measurements.

samples containing designated concentrations of PD-1 (100 fg/mL to 1 ng/mL), PD-L1 (50 fg/mL to 100 pg/mL), and LAG-3 (100 fg/mL to 1 ng/mL) were separately driven through the device under the applied ac-EHD field. Blank serum samples without target fortification (0 fg/mL) served as the negative controls. The left panel of Fig. 4 shows the representative overlaid SERS spectra from the different concentrations of (a) PD-1, (c) PD-L1, and (e) LAG-3. As the target concentration increased, the intensity of the SERS signal increased proportionally. The right panel of Fig. 4 shows the dynamic range for (b) PD-1, (d) PD-L1, and (f) LAG-3. For the dynamic range, the average peak Raman intensity (n = 3) at 1074 cm^{-1} for PD-1, 1337 cm^{-1} for PD-L1, and 1174 cm^{-1} for LAG-3 was plotted as a function of target concentration. The corresponding line relation between protein concentration and SERS intensity response curve for PD-1, PD-L1 and LAG-3 immune checkpoint marker proteins has been shown in Supplementary Fig. S7(a)-(c). It shows the consistency in the functioning of device with coefficient of determination (R^2) of PD-1 (0.992), PD-L1 (0.989) and LAG-3 (0.994), respectively. The assay covered a dynamic range of 2–4 orders of magnitude with detection limits as low as 50 fg/mL (for PD-L1). Furthermore, the assay was highly reproducible with errors < 3.65% RSD. These assay performance values are well suited for trace level detection of immune checkpoint markers. For instance, small changes in serum PD-L1 served as a predictive biomarker for the outcome of immune checkpoint blockade therapy in malignant melanoma and aggressive diffuse large B-Cell lymphoma (Rossille et al., 2014; Zhou et al., 2017). However, the detection of these small changes could be a challenge for standard ELISA technology. This is because ELISA based technology is often limited by non-specific binding and long assay time (4 h). This situation becomes aggravated for samples with very low target concentrations that can result false-positive signal. An advantage of our assay is that it used ac-EHD fluid flow to reduce the non-specific binding and minimize the chances for false positive results. Recently,

Chou et al. reported a microfluidic platform with fluorescence readout which achieved highly sensitive detection of PD-L1 in the picomolar range (Chou et al., 2018). However, fluorescence based assays are limited by high background signal due to photo-bleaching and difficult for multiplexing due to spectral overlapping. On the contrary, our SERS-microfluidic assays provided highly sensitive detection with multiplexing capability which may address the limitations associated with current technologies.

3.5. Multiplex immune checkpoint detection

To demonstrate the potential clinical application of our assay for parallel immune checkpoint detection, healthy serum samples fortified with the three immune checkpoint markers were analysed. To integrate the multiplexed detection, the channels of the device were functionalised with anti-PD-1, anti-PD-L1, and anti-LAG-3 NY-scFvs. The fortified serum samples and control samples (blank serum without spiking) were then run through the device under the optimized ac-EHD conditions. After target capture, the detection was facilitated by incubation with the SERS nanotag solution under ac-EHD conditions. The SERS nanotag solution contained the anti-PD-1, anti-PD-Ll, and anti-LAG-3 antibodies conjugated SERS nanoparticle or barcodes for individual target identification. The representative SERS spectra and corresponding false-colour images are shown in Fig. 5(a) and (b), respectively. The narrow spectral width of the SERS reporter provided clear and multiplexed target identification without spectral overlap. The high detection sensitivity using SERS readout and reduction of non-specific adsorption due to ac-EHD were crucial for improving the assay performance. These were key two features in achieving detection limits of 100 fg/mL of protein from complex biological sample.

To better understand the assay performance, we have compared our assay with previously developed method for immune checkpoint detection (Table 1) in terms of sensitivity and dynamic detection range. We have compared the sensing parameters (detection limit and dynamic range) of the standard methods like ELISA (which can quantify the protein concentration) whereas IHC (Immunohistochemistry) and western blot methods were not considered as they are less sensitive and require high concentrations of protein. As shown in Table 1, our method has similar sensitivity like ELISA, however, has better dynamic range with low detection limit up to 100 fg/mL. Moreover, our SERS ac-EHD method provides significant advantages over fluorescence based ELISA techniques due to greater multiplexing capabilities and photostability.

Finally, we investigated the storage stability of our microfluidic device after 0–4 weeks of storage in a vacuum sealed box. We performed the assay for the detection of 1 ng/mL PD-1 in each device

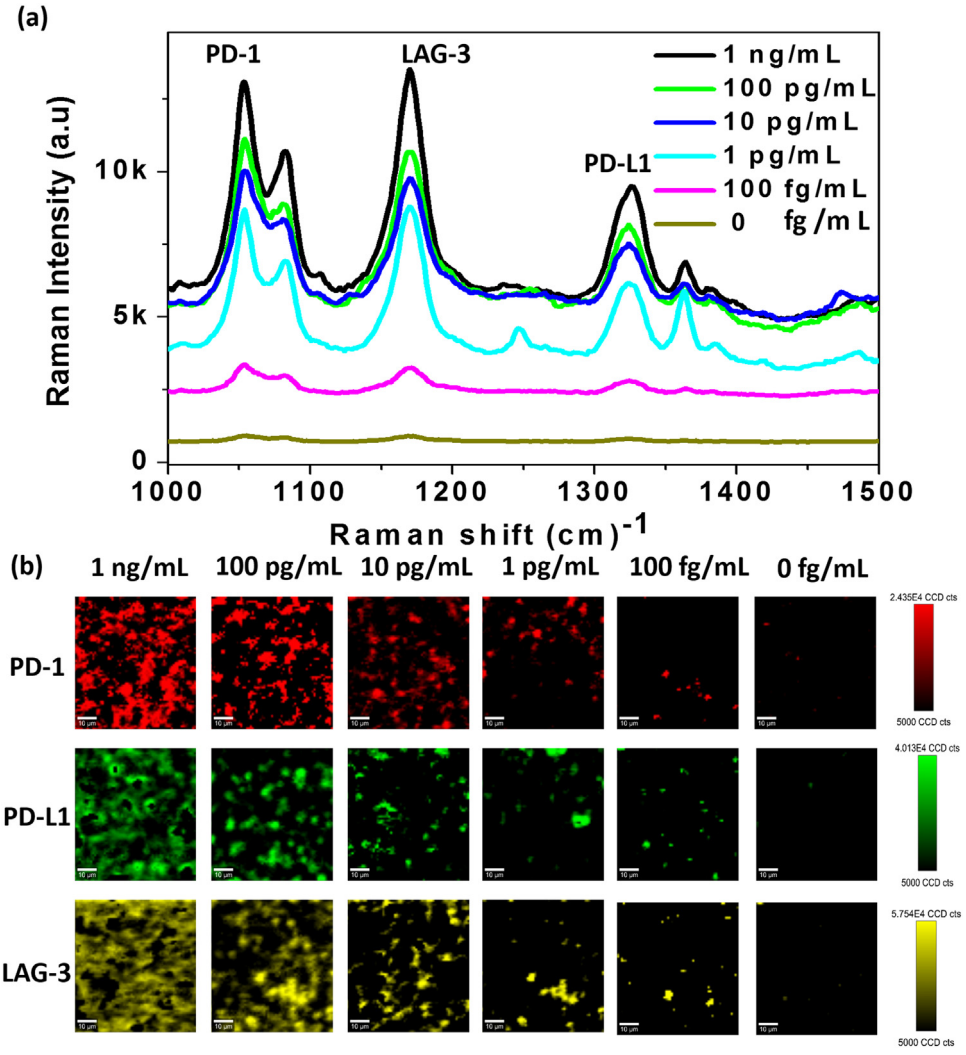

Fig. 5. (a) Typical SERS spectra of the parallel detection of PD-1, PD-L1, and LAG-3 in serum samples under ac-EHD field (f = 1.1 kHz and V_{pp} = 120 mV). (b) false colour SERS images (scale bar is 10 μm) for PD-1 (red), PD-L1 (green) and LAG-3 (yellow) detection in the concentration range from 1 ng/mL to 100 fg/mL spiked in serum samples. Control experiments were performed using blank serum samples (0 fg/mL). (For interpretation of the references to color in this figure legend, the reader is referred to the web version of this article.).

Table 1
Comparison table of the most recent literatures working towards detection of immune checkpoints.

Technique	LOD	Range	Reference
ELISA	PD-1:0.117 ng/mL PD-L1:0.012 ng/mL LAG-3: N/A	PD-1: 0.038–25.93 ng/mL) PD-L1: 0.007–0.632 ng/mL LAG-3: N/A	(Kruger et al., 2017)
ELISA	PD-L1: 130fM PD-1: N/A LAG-3: N/A	PD-1: N/A PD-L1: 0.13–130 p.M. LAG-3: N/A	(Chou et al., 2018)
ELISA	PD-1:0.117 pg/mL PD-L1: 150 pg/mL LAG-3: N/A	PD-1: 117–380 pg/mL) PD-L1: 150–850 pg/mL LAG-3: N/A	(Li et al., 2016)
ELISA	PD-1: 20 pg/mL PD-L1: 3.9 pg/mL LAG-3: N/A	PD-1: 20 – 517 pg/mL PD-L1: 3.9–398 pg/mL LAG-3: N/A	(Yanaba et al., 2016)
SERS	PD-1: 6.17 pg/mL PD-L1: 0.68 pg/mL EGFR: 69.86 pg/mL	PD-1: 0.01 – 1.0 ng/mL PD-L1: 0.001–10 ng/mL EGFR: 0.1–1000 ng/mL	(Li et al., 2018)
SERS- ac-EHD (chip)	PD-1: 100 fg/mL PD-L1: 50 fg/mL LAG-3: 100fg/mL	PD-1: 100 fg/mL – 1 ng/mL PD-L1:50 fg/mL – 100 pg/mL LAG-3: 100 fg/mL – 1 ng/mL	Our work

stored for 0–4 weeks and measured the signal intensity. Supplementary Fig. S8 shows the SERS signal intensity as a function of storage time. The signal intensities were comparable over the tested storage period which demonstrates a good assay reproducibility as well as excellent storage stability.

4. Conclusions

In summary, we have developed an immune checkpoint biosensing strategy that combines SERS spectral encoding on an ac-EHD device for multiplexed and sensitive detection of soluble PD-1, PD-L1 and LAG-3. The significance of our research approach is the first demonstration of chip-based assay for the simultaneous detection of three immune checkpoint markers using SERS barcoding. We also explored the strategy of utilizing the novel recombinant NY-scFv affinity reagents for capturing target on the graphene oxide modified electrodes of the ac-EHD device. The ac-EHD fluid flow actively stimulated target-NY-scFv collisions and reduced the non-specific sensor binding. Three SERS reporters were applied to unambiguously identify the captured immune checkpoint markers. These features were key in enabling the multiplexed target detection in human serum samples with a sensitivity of 100 fg/mL. The immune checkpoint device could analyse five samples in parallel with a turn-around time of 45 min. Moreover, this microfluidic chip is rapid, multiplexable, highly sensitive and specific and can be used for the analysis of other clinically relevant biomarkers such as DNA/RNA, exosomes, circulating free DNA, etc. As a proof-of-concept study, this method is limited to the detection of three immune checkpoints at this stage. However, we believe that by increasing the multiplexing capability of the device, it would be possible to generate a holistic immune profile by monitoring a large number of immune checkpoint markers which will strongly support personalised cancer immunotherapy monitoring.

Acknowledgement

The authors would like to acknowledge the financial support by the National Breast Cancer Foundation of Australia (CG-12-07) for this project. K.K.R would like to acknowledge the financial support from the Australian Government Research Training Program scholarship. AW thanks the University of Queensland Development Fellowship (UQFEL1831057). We would like to thank Junrong Li for the SEM study of the electrodes. The authors also acknowledge the facility support from the Australian National Fabrication Facility-Queensland Node (ANFF-Q) in The University of Queensland.

Supporting information

Supporting Information is available from the publisher or from the author.

Appendix A. Supporting information

Supplementary data associated with this article can be found in the online version at doi:10.1016/j.bios.2018.10.044.

References

Ali, M.A., Kamil Reza, K., Srivastava, S., Agrawal, V.V., John, R., Malhotra, B.D., 2014. Langmuir 30 (14), 4192–4201.
Alme, A.K., Karir, B.S., Faltas, B.M., Drake, C.G., 2016. Urologic Oncology: Seminars and Original Investigations. Elsevier, pp. 171–181.
Anderson, A.C., Joller, N., Kuchroo, V.K., 2016. Immunity 44 (5), 989–1004.
Chen, D., Feng, H., Li, J., 2012. Chem. Rev. 112.
Chou, C.-.K., Huang, P.-.J., Tsou, P.-.H., Wei, Y., Lee, H.-.H., Wang, Y.-.N., Liu, Y.-.L., Shi, C., Yeh, H.-.C., Kameoka, J., 2018. Biosens. Bioelectron.
Frens, G., 1973. Nature 241 (105), 20–22.
Grewal, Y.S., Shiddiky, M.J., Mahler, S.M., Cangelosi, G.A., Trau, M., 2016. ACS Appl. Mater. Interfaces 8 (45), 30649–30664.
Grewal, Y.S., Shiddiky, M.J., Spadafora, L.J., Cangelosi, G.A., Trau, M., 2015. J. Phys. Chem. C 119 (22), 12674–12680.
Holliger, P., Hudson, P.J., 2005. Nat. Biotechnol. 23 (9), 1126.
Huang, J.A., Zhang, Y.L., Ding, H., Sun, H.B., 2015a. Adv. Opt. Mater. 3 (5), 618–633.
Huang, R.-Y., Eppolito, C., Lele, S., Shrikant, P., Matsuzaki, J., Odunsi, K., 2015b. Oncotarget 6 (29), 27359–27377.
Iwai, Y., Ishida, M., Tanaka, Y., Okazaki, T., Honjo, T., Minato, N., 2002. Proc. Natl. Acad. Sci. USA 99 (19), 12293–12297.
Joller, N., Peters, A., Anderson, A.C., Kuchroo, V.K., 2012. Immun. Rev. 248 (1), 122–139.
Kamil Reza, K., Wang, J., Vaidyanathan, R., Dey, S., Wang, Y., Trau, M., 2017. Small 13 (9), 1602902.
Karin, M., Lawrence, T., Nizet, V., 2006. Cell 124 (4), 823–835.
Koyama, S., Akbay, E.A., Li, Y.Y., Herter-Sprie, G.S., Buczkowski, K.A., Richards, W.G., Gandhi, L., Redig, A.J., Rodig, S.J., Asahina, H., 2016. Nat. Commun. 7, 10501.
Kruger, S., Legenstein, M.-L., Rösgen, V., Haas, M., Modest, D.P., Westphalen, C.B., Ormanns, S., Kirchner, T., Heinemann, V., Holdenrieder, S., 2017. Oncoimmunology 6 (5), e1310358.
Laing, S., Gracie, K., Faulds, K., 2016. Chem. Soc. Rev. 45 (7), 1901–1918.
Li, J., Wang, J., Grewal, Y.S., Howard, C.B., Raftery, L.J., Mahler, S., Wang, Y., Trau, M., 2018. Anal. Chem. 90 (17), 10377–10384.
Li, Y., Xiao, Y., Su, M., Zhang, R., Ding, J., Hao, X., Ma, Y., 2016. Exp. Ther. Med. 11 (1), 251–256.
Luo, S.-C., Sivashanmugan, K., Liao, J.-D., Yao, C.-K., Peng, H.-C., 2014. Biosens. Bioelectron. 61, 232–240.
Nagato, T., Ohkuri, T., Ohara, K., Hirata, Y., Kishibe, K., Komabayashi, Y., Ueda, S., Takahara, M., Kumai, T., Ishibashi, K., 2017. Cancer Immunol., Immunother. 66 (7), 877–890.
Pardoll, D.M., 2012. Nat. Rev. Cancer 12 (4), 252.
Postow, M.A., Callahan, M.K., Wolchok, J.D., 2015. J. Clin. Oncol. 33 (17), 1974–1982.
Pumera, M., 2011. Mater. Today 14 (7–8), 308–315.
Qian, X.-M., Nie, S., 2008. Chem. Soc. Rev. 37 (5), 912–920.

Reza, K.K., Ali, M.A., Srivastava, S., Agrawal, V.V., Biradar, A., 2015. Biosens. Bioelectron. 74, 644–651.
Rossille, D., Gressier, M., Damotte, D., Maucort-Boulch, D., Pangault, C., Semana, G., Le Gouill, S., Haioun, C., Tarte, K., Lamy, T., 2014. Leukemia 28 (12), 2367.
Sakaguchi, S., 2004. Annu. Rev. Immunol. 22, 531–562.
Scott, A.M., Wolchok, J.D., Old, L.J., 2012. Nat. Rev. Cancer 12 (4), 278.
Sharma, P., Allison, J.P., 2015. Cell 161 (2), 205–214.
Shi, M., Xing, Y., Zhang, Z., Huang, J., Chen, Y., 2013. Zhonghua Zhong Liu Za Zhi Chin. J. Oncol.) 35 (2), 85–88.
Vaidyanathan, R., Rauf, S., Grewal, Y.S., Spadafora, L.J., Shiddiky, M.J., Cangelosi, G.A., Trau, M., 2015. Anal. Chem. 87 (23), 11673–11681.
Wang, Y., Li, Z., Wang, J., Li, J., Lin, Y., 2011. Trends Biotechnol. 29 (5), 205–212.
Wang, Y., Rauf, S., Grewal, Y.S., Spadafora, L.J., Shiddiky, M.J., Cangelosi, G.A., Schlücker, S., Trau, M., 2014. Anal. Chem. 86 (19), 9930–9938.
Wang, Y., Vaidyanathan, R., Shiddiky, M.J.A., Trau, M., 2015. ACS Nano 9 (6), 6354–6362.
Wang, Z., Zong, S., Wu, L., Zhu, D., Cui, Y., 2017. Chem. Rev. 117 (12), 7910–7963.
Wherry, E.J., 2011. T Cell Exhaust. Nat. Immun. 12 (6), 492.
Yanaba, K., Hayashi, M., Yoshihara, Y., Nakagawa, H., 2016. J. Dermat. 43 (8), 954–957.
Yang, S., Xu, B., Zhang, J., Huang, X., Ye, J., Yu, C., 2010. J. Phys. Chem. C 114 (10), 4389–4393.
Zeman, E.J., Schatz, G.C., 1987. J. Phys. Chem. 91 (3), 634–643.
Zhao, J., Lui, H., McLean, D.I., Zeng, H., 2007. Appl. Spectrosc. 61 (11), 1225–1232.
Zhou, J., Mahoney, K.M., Giobbie-Hurder, A., Zhao, F., Lee, S., Liao, X., Rodig, S., Li, J., Wu, X., Butterfield, L.H., 2017. Cancer Immun. Res. 0329, 2016.